Palaeogeography, Palaeoclimatology, Palaeoecology 284 (2009) 295–314

Contents lists available at ScienceDirect

Palaeogeography, Palaeoclimatology, Palaeoecology

journal homepage: www.elsevier.com/locate/palaeo

Environmental impact of the 73 ka Toba super-eruption in South Asia

Martin A.J. Williams [a,*], Stanley H. Ambrose [b], Sander van der Kaars [c,1], Carsten Ruehlemann [d], Umesh Chattopadhyaya [e], Jagannath Pal [e], Parth R. Chauhan [f]

[a] Geographical & Environmental Studies, University of Adelaide, Adelaide 5005, Australia
[b] Department of Anthropology, University of Illinois, Urbana IL 61801, USA
[c] Centre for Palynology and Palaeoecology, School of Geography and Environmental Science, Monash University, Clayton, Victoria 3168, Australia
[d] Bundesanstalt für Geowissenschaften und Rohstoffe, Referat B3.23/ Meeresgeologie und Tiefseebergbau, Stillweg 2, 30655 Hannover, Germany
[e] Department of Ancient History, Culture and Archaeology, University of Allahabad, Allahabad 211002, India
[f] Stone Age Institute and CRAFT Research Center, Indiana University, Bloomington, IN 47408, USA

ARTICLE INFO

Article history:
Received 2 November 2008
Received in revised form 6 October 2009
Accepted 8 October 2009
Available online 29 October 2009

Keywords:
Carbon isotopes
Indian Ocean
Marine cores
Palaeoclimate
Pollen analysis
Soil carbonate
Tephra
Toba volcano

ABSTRACT

The cooling effects of historic volcanic eruptions on world climate are well known but the impacts of even bigger prehistoric eruptions are still shrouded in mystery. The eruption of Toba volcano in northern Sumatra some 73,000 years ago was the largest explosive eruption of the past two million years, with a Volcanic Explosivity Index of magnitude 8, but its impact on climate has been controversial. In order to resolve this issue, we have analysed pollen from a marine core in the Bay of Bengal with stratified Toba ash, and the carbon isotopic composition of soil carbonates directly above and below the ash in three sites on a 400 km transect across central India. Pollen evidence shows that the eruption was followed by initial cooling and prolonged desiccation, reflected in a decline in tree cover in India and the adjacent region. Carbon isotopes show that C_3 forest was replaced by wooded to open C_4 grassland in central India. Our results demonstrate that the Toba eruption caused climatic cooling and prolonged deforestation in South Asia, and challenge claims of minimal impact on tropical ecosystems and human populations.

1. Introduction

The ~73 ka eruption of the Toba volcano in northern Sumatra was the largest explosive eruption of the Quaternary (Ninkovich et al., 1978a,b; Chesner et al., 1991) and produced ca. 2500–3000 km^3 of dense rock equivalent of pyroclastic ejecta (Rose and Chesner, 1987; Gates and Ritchie, 2007, p. 259) compared to the 100–200 km^3 from the 1815 Tambora eruption (Rampino and Self, 1982; De Silva, 2008). The Volcanic Explosivity Index (VEI) of the Toba super-eruption is 8, or an order of magnitude larger than the Tambora VEI of 7 (Gates and Ritchie, 2007, p. 259; De Silva, 2008). The VEI denotes the magnitude of an eruption based on a combination of erupted tephra volume and eruption plume height (De Silva, 2008).

The Youngest Toba Tuff (YTT) is found across peninsular India and in the Indian Ocean (Ninkovich et al., 1978a; Westgate et al., 1998). It provides an isochronous marker in sedimentary sequences with fossil soils and in deep sea cores that can be directly correlated with the global climatic records in polar ice cores.

Volcanic sulfate from the Greenland ice core at ~73 ka (Zielinski et al., 1996) supports the hypothesis proposed by Rampino and Self (1992) that the Toba eruption caused a six-year volcanic winter . This sulfate spike also marks the abrupt onset of an 1800-year period of the coldest temperatures of the last 125,000 years (Zielinski et al., 1996; Lang et al., 1999; North Greenland Ice Project Members, 2004). This instant ice age corresponds to the stadial (cold) half of Dansgaard–Oeschger (D–O) cycle 20, which is the coldest of 23 abrupt stadial–interstadial cycles between 100 ka and 15 ka (Grootes et al., 1993; Dansgaard et al., 1993). The magnitude of the climate impact of the Toba eruption has been questioned because of uncertainties in estimates of stratospheric sulfate (Oppenheimer, 2002). However, most models of the climatic impact of the massive stratospheric sulfate loading following the Toba super-eruption (Bekki et al., 1996; Jones et al., 2005; Robock et al., 2009) indicate that it may have enhanced global cooling, particularly during the first two centuries following this eruption (Zielinski et al., 1996). Global cooling may have been enhanced by increasing terrestrial albedo over India from the ash blanket (Jones et al., 2007).

There has been a great deal of speculation about the possible impact of the ~73 ka Toba super-eruption upon world climate and upon human populations (Rampino et al., 1985; Ambrose, 1998; Rampino and Ambrose, 2000). Genetic evidence points to a sudden drop in numbers

* Corresponding author.
E-mail address: martin.williams@adelaide.edu.au (M.A.J. Williams).
[1] Present address: Department of Palynology and Climate Dynamics, Albrecht-von-Haller-Institute for Plant Sciences, University of Göttingen, Untere Karspüle 2, 37073 Göttingen, Germany.

0031-0182/$ – see front matter © 2009 Elsevier B.V. All rights reserved.
doi:10.1016/j.palaeo.2009.10.009

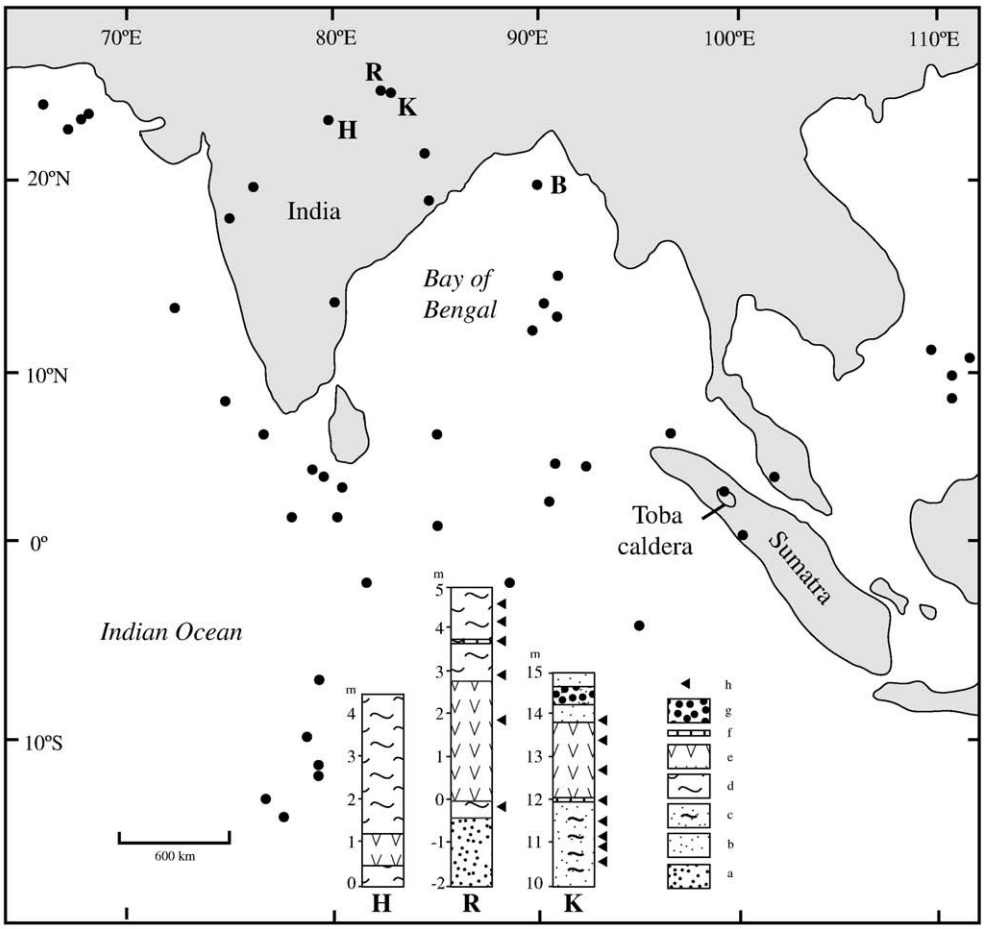

Fig. 1. Distribution of volcanic ash from the 73 ka Toba super-eruption showing location of marine cores and sections sampled in India. Black dots represent Toba tephra occurrences on land and in marine cores. R is site of first Toba ash discovery at Son–Rehi confluence. B is marine core S0188-342KL in the Bay of Bengal; K is Khunteli; R is Rehi; H is Hirapur. Key to stratigraphic sections in India: a is coarse sand; b is medium/fine sand; *c* is silt loam/sandy loam/interstratified sand and loam; *d* is clay; e is Toba volcanic ash; *f* is massive carbonate; and *g* is gravel; *h* is sampled pedogenic carbonate horizon.

of the ancestors of living human populations to a few thousand at about this time (Haigh and Maynard Smith, 1972; Harpending et al., 1993; Jorde et al., 1998), with the survivors possibly concentrated in equatorial African biotic refugia (Ambrose, 1998; Tishkoff et al., 2009). Modern humans may have expanded to Asia and Europe some time after this eruption, arriving in Australia by 50 ka (Bowler et al., 2003) and western Eurasia by 40–45 ka (Forster, 2004; Mellars, 2006; Richter et al., 2008), but the date of expansion to Asia relative to the eruption (Petraglia et al., 2007) and its impact on human populations has been contested (Gathorne-Hardy and Harcourt-Smith, 2003; Scholz et al., 2007; Cohen et al., 2007). Despite the magnitude of the 73 ka Toba eruption, its impact on regional and global climate has remained controversial, with current views polarised into those who have argued on geological and ice core geochemical evidence for a substantial impact (Rampino and Self, 1992, 1993; Zielinski et al., 1996; Ambrose, 1998; Rampino and Ambrose, 2000) and those who argue for minimal or no impact based on sea surface temperature estimates (Schulz et al., 2002), termite survival (Gathorne-Hardy and Harcourt-Smith, 2003; see reply by Ambrose,

Table 1
Particle size distribution of the YTT ash at the Rehi section, Son valley, India. Particle size was determined by laser scatter analysis.

Sample	Lab ID[a]	Height above base of ash (cm)	Calculation range (μm)	Diameter Median (μm)	Mode (μm)	Mean (μm)	Coefficient of variation %	Standard deviation
S54	S54/280,140ud	65	2.84–178.2	39.85	45.45	45.66	59.1	27.01
S54	S54/280,140,70d	65	1.42–170.9	36.24	38.63	40.14	54.8	21.99
S54	S54/280,140d	65	2.84–170.9	36.35	42.13	40.33	54.2	21.86
S58	S58/280,140d	105	2.84–103.8	28.50	29.70	30.55	49.3	15.07
S60	S60/280,140ud	125	2.84–191.0	52.56	58.00	60.31	59.5	35.90
S60	S60/280,140d	125	2.84–191.0	41.59	52.12	46.65	62.4	29.12
S64	S64/280,140d	250	2.84–191.0	39.06	50.44	42.27	52.4	22.16
S65	S65/280,140d	280	2.84–138.8	34.53	58.41	38.19	59.3	22.63
S66	S66/280,140ud	310	2.84–155.1	32.40	35.99	35.82	59.4	21.27
S66	S66/280,140d	310	2.84–183.2	44.24	52.74	54.28	70.7	38.40
		Mean		38.53	46.36	43.42	58.12	25.54
		Standard deviation		6.71	9.63	8.76	5.96	7.16

ud = undispersed.
[a] d = dispersed.

Table 2
Provenance, description, weight% loss from heating, weight% carbonate carbon, and d^{13}C‰$_{PDB}$ and d^{18}O‰$_{PDB}$ values of carbonate nodules and root-casts from localities with Toba ash on the Son and Narmada rivers, central India.

Field #	Location	Trench	Level	Depth cm[a]	Description	% Loss [b]	Wt%C[c]	δ^{13}C‰	∂^{18}O‰
SON05–01A	Khunteli	1	2	−172	Rootcast	1.7	4.32	−11.98	−6.92
SON05-01B	Khunteli	1	2	−172	Rootcast	1.5	2.44	−9.71	−4.26
SON05-01C	Khunteli	1	2	−171	Rootcast	0.9	6.64	−12.24	−7.00
SON05-01D	Khunteli	1	2	−171	Nodule	1.7	2.93	−10.79	−5.51
SON05-01E	Khunteli	1	2	−170	Nodule	1.6	3.40	−11.89	−6.66
SON05-01F	Khunteli	1	2	−170	Rootcast	0.9	5.88	−11.56	−6.12
SON05-02A	Khunteli	1	3	−107	Nodule	1.6	5.47	−12.36	−6.99
SON05-02B	Khunteli	1	3	−106	Nodule	1.2	3.58	−12.25	−7.14
SON05-02C	Khunteli	1	3	−105	Nodule	1.2	7.61	−12.58	−6.59
SON05-03A	Khunteli	1	4	−94	Rootcast	1.9	7.50	−12.20	−6.78
SON05-03B	Khunteli	1	4	−94	Nodule	1.9	3.14	−11.82	−6.39
SON05-03C	Khunteli	1	4	−93	Rootcast	0.3	3.28	−12.35	−6.81
SON05-04	Khunteli	1	6	−67	Rootcast	1.2	4.26	−11.95	−6.77
SON05-05A	Khunteli	1	8	−5	Platy lamina	2.7	6.08	−11.99	−6.73
SON05-05B	Khunteli	1	8	−4	Platy lamina	2.3	6.99	−12.14	−6.38
SON05-05C	Khunteli	1	8	−4	Nodule	1.5	6.02	−12.10	−6.98
SON05-05D	Khunteli	1	8	−3	Rootcast	3.2	5.16	−12.23	−7.21
SON05-10	Khunteli	1	9	30	Toba ash	4.9	0.00		
SON05-06A[d]	Khunteli	1	9	47	Crack fill	2.8	3.92	−12.70	−7.34
SON05-06B[d]	Khunteli	1	9	54	Crack fill	2.1	6.78	−12.87	−7.04
SON05-07A	Khunteli	1	9	126	Nodule	2.2	3.99	−3.76	−5.18
SON05-07B	Khunteli	1	9	127	Nodule	2.1	4.01	−12.75	−6.60
SON05-07C	Khunteli	1	9	127	Nodule	0.8	6.29	−6.54	−5.47
SON05−07D	Khunteli	1	9	128	Nodule	0.8	4.36	−2.02	−4.43
SON05-07E	Khunteli	1	9	128	Rootcast	0.7	5.65	−5.75	−4.92
SON05-07F	Khunteli	1	9	129	Rootcast	1.2	3.94	−11.34	−6.82
SON05-07G	Khunteli	1	9	129	Rootcast	1.5	5.02	−7.39	−5.69
SON05-08A	Khunteli	1	9	170	Rootcast	2.6	4.44	−2.25	−6.17
SON05-08B[d]	Khunteli	1	9	170	Crack fill	2.4	4.01	−12.16	−7.03
SON05-08C	Khunteli	1	9	170	Nodule	3.0	3.76	−4.94	−6.51
SON05-09A	Khunteli	1	10	183	Nodule	4.4	2.91	−12.22	−6.89
SON05-09B	Khunteli	1	10	183	Nodule	4.7	4.62	−12.40	−7.02
SON05-09C	Khunteli	1	10	183	Nodule	2.7	4.04	−12.16	−6.91
SON05-09D	Khunteli	1	10	183	Nodule	2.4	5.80	−12.76	−7.30
SON05-09E	Khunteli	1	10	183	Nodule	3.2	3.95	−3.18	−5.35
SON05-09F	Khunteli	1	10	183	Nodule	2.5	2.55	−12.56	−6.73
SON05-09G	Khunteli	1	10	183	Rootcast	1.7	4.07	−12.00	−6.84
SON05-18G	Rehi	2	8	−23	Nodule	1.4	2.77	−10.21	−6.26
SON05-18F	Rehi	2	8	−20	Nodule	1.5	6.70	−3.50	−5.39
SON05-18E	Rehi	2	8	−17	Nodule	2.2	6.44	−10.20	−6.31
SON05-18D	Rehi	2	8	−13	Nodule	1.6	7.01	−10.23	−6.32
SON05-18C	Rehi	2	8	−10	Nodule	1.4	3.83	−10.39	−6.51
SON05-18B	Rehi	2	8	−7	Nodule	1.3	6.60	−10.20	−6.22
SON05-18A	Rehi	2	8	−4	Nodule	2.3	4.43	−10.25	−6.42
SON05-11A[e]	Rehi	1	1	−10	Nodule	2.1	3.59	−4.14	−4.51
SON05-11B[e]	Rehi	1	1	−10	Nodule	2.0	5.16	−10.51	−6.67
SON05-12	Rehi	1	3	37	Toba ash	7.6	0.00		
SON05-17E	Rehi	2	5	176	Rootcast	2.2	4.13	−10.01	−5.60
SON05-17D	Rehi	2	5	178	Nodule	2.9	6.66	−4.39	−5.16
SON05-17C	Rehi	2	5	180	Nodule	0.4	3.83	−4.99	−5.19
SON05-17B	Rehi	2	5	182	Nodule	2.2	7.30	−4.50	−5.63
SON05-17A	Rehi	2	5	184	Nodule	1.7	6.50	−3.97	−5.28
SON05-16G	Rehi	2	3	382	Nodule	2.3	6.19	−0.67	−6.21
SON05-16E	Rehi	2	3	391	Nodule	2.7	4.54	−5.35	−5.16
SON05-16F	Rehi	2	3	391	Nodule	2.2	4.94	0.32	−7.00
SON05-16C	Rehi	2	3	392	Nodule	2.1	5.48	0.50	−6.88
SON05-16D	Rehi	2	3	392	Nodule	2.6	4.69	−0.67	−6.87
SON05-16A	Rehi	2	3	393	Calcrete	1.2	5.35	−4.80	−5.85
SON05-16B	Rehi	2	3	393	Nodule	2.1	2.89	−3.63	−5.65
SON05-15F	Rehi	2	2	412	Nodule	1.5	8.57	−9.63	−3.37
SON05-15E	Rehi	2	2	413	Rootcast	0.9	5.18	−4.30	−5.48
SON05-15D	Rehi	2	2	414	Nodule	1.1	7.50	−9.77	−3.38
SON05-15C	Rehi	2	2	415	Nodule	1.1	6.90	−9.55	−3.34
SON05-15B	Rehi	2	2	416	Nodule	1.5	6.84	−8.84	−3.10
SON05-15A	Rehi	2	2	417	Nodule	1.5	6.43	−9.15	−3.55
SON05-14D	Rehi	2	2	450	Nodule	2.0	5.63	−5.74	−4.56
SON05-14E	Rehi	2	2	450	Nodule	1.4	7.26	−9.54	−3.64
SON05-14B	Rehi	2	2	451	Nodule	1.6	2.98	−8.33	−4.02
SON05-14C	Rehi	2	2	451	Nodule	1.7	7.18	−8.87	−3.44
SON05-14A	Rehi	2	2	452	Nodule	2.3	8.50	−9.45	−3.07
SON05-13F	Rehi	2	1	479	Nodule	2.5	7.77	−4.79	−5.71
SON05-13D	Rehi	2	1	480	Nodule	1.5	6.91	−8.10	−6.16
SON05-13E	Rehi	2	1	480	Nodule	1.7	7.39	−7.87	−5.95

(continued on next page)

Table 2 (*continued*)

Field #	Location	Trench	Level	Depth cm[a]	Description	% Loss [b]	Wt%C[c]	δ^{13}C‰	∂^{18}O‰
SON05-13B	Rehi	2	1	481	Nodule	2.7	7.12	−4.66	−5.40
SON05-13C	Rehi	2	1	481	Nodule	2.8	6.76	−5.43	−5.53
SON05-13A	Rehi	2	1	482	Nodule	2.6	6.88	−4.37	−5.31
SON05-19A	Hirapur	1	3	45	Nodule	4.6	7.17	−6.08	−4.15
SON05-19B	Hirapur	1	3	44	Nodule	4.6	6.73	−6.27	−4.19
SON05-19C	Hirapur	1	3	44	Nodule	3.5	9.40	−6.08	−4.18
SON05-19D	Hirapur	1	3	43	Nodule	3.5	7.24	−6.34	−4.01
SON05-19E	Hirapur	1	3	43	Nodule	9.5	8.21	−6.65	−4.31
SON05-19F	Hirapur	1	3	42	Nodule	4.7	5.93	−6.31	−4.33
SON05-20A	Hirapur	2	1	109	Rootcast	3.3	5.98	−9.71	−5.38
SON05-20B	Hirapur	2	1	108	Rootcast	2.7	9.83	−10.00	−4.94
SON05-20C	Hirapur	2	1	108	Rootcast	3.4	8.83	−10.16	−4.91
SON05-20D	Hirapur	2	1	107	Nodule	3.3	8.31	−10.01	−4.97
SON05-20E	Hirapur	2	1	107	Nodule	3.1	8.85	−9.82	−4.73
SON05-21A	Hirapur	2	1	87	Rootcast	4.3	6.57	−10.01	−4.94
SON05-21B	Hirapur	2	1	87	Nodule	3.5	5.15	−10.09	−4.80
SON05-21C	Hirapur	2	1	87	Nodule	5.1	5.89	−10.27	−5.36
SON05-21D	Hirapur	2	1	87	Nodule	5.2	6.47	−9.97	−4.95
SON05-21E	Hirapur	2	1	87	Nodule	4.4	8.86	−9.90	−5.24
SON05-22A	Hirapur	2	3	−22	Nodule	2.7	8.61	−9.82	−4.98
SON05-22B	Hirapur	2	3	−23	Rootcast	3.4	6.92	−9.57	−5.36
SON05-22C	Hirapur	2	3	−24	Rootcast	3.5	8.10	−10.01	−5.19
SON05-22D	Hirapur	2	3	−25	Rootcast	2.7	7.95	−10.07	−5.06
SON05-22E	Hirapur	2	3	−26	Nodule	4.4	7.64	−9.53	−5.06
SON05-22F	Hirapur	2	3	−27	Nodule	4.0	8.57	−9.62	−5.03
SON05-22G	Hirapur	2	3	−28	Nodule	4.7	7.27	−9.46	−4.85

[a] Depth below or height (cm) above base of volcanic ash.
[b] Weight% loss after roasting under vacuum at 380 °C.
[c] Weight% carbonate carbon. Pure $CaCO_3$ is ~12% C.
[d] Samples excluded from analysis because they fill cracks in the sediment and thus post-date sedimentation and soil formation. Their low δ^{13}C values indicate they formed in a pure C_3 floral habitat.
[e] Samples excluded from analysis because they formed in coarse laminated sandstone, probably of fluvial origin.

2003), archaeological evidence (Petraglia et al., 2007) and an earlier candidate for a climatic disaster (Cohen et al., 2007). This debate is doomed to remain sterile until unequivocal evidence is available documenting the possible impact of the Toba eruption upon terrestrial ecosystems. We here report the results of two independent lines of enquiry into the impact of this eruption on ecosystems in and near to India. Stable carbon isotopic analyses of fossil soil carbonates directly beneath and above the Toba ash from sites in the Son and Narmada valleys of central India, located ~3400 km NW of Toba, indicate a change from forests before the Toba eruption to open or wooded grassland ecosystems after the eruption. Pollen grains extracted from samples collected immediately beneath and above the Toba ash from a marine core, in the Bay of Bengal, show a reduction in tree cover and cooling followed by prolonged drought. Our results provide the first direct terrestrial evidence of a significant regional environmental impact of the Toba eruption.

We hypothesise that other tropical ecosystems may also have been affected by the Toba super-eruption and subsequent 1800-year-long stadial. Genetic bottlenecks in humans and other species (Goldberg, 1996; Ambrose, 1998; Luo et al., 2004; Steiper, 2006; Thalmann et al., 2007; Hernandez et al., 2007), and the regional extinction of 12 southeast Asian large mammal species (Louys, 2007), may have been initiated by this event, and the course of modern human evolution and dispersals may have been affected by the environmental impact of the Toba eruption (Ambrose, 2002, 2006).

2. Distribution of the 73 ka Toba ash

Ash from the 73 ka Toba eruption is widespread across the Bay of Bengal (Rose and Chesner, 1987), crops out as channel fill or valley-floor deposits across peninsular India (Acharyya and Basu, 1993; Shane et al., 1995; Westgate et al., 1998), and is present in marine sediment cores from the Indian Ocean, the Arabian Sea and the East China Sea (Pattan et al., 1999; Song et al., 2000; Bühring et al., 2000; Liu et al., 2006) (Fig. 1).

Williams and Royce (1982) were the first to discover Quaternary volcanic ash in India, at the Son–Rehi confluence (Fig. 1; Table 1) where ash from the 73 ka Toba eruption fills a buried channel 3 m deep and 10 m wide (Williams and Clarke, 1984, 1995; Williams et al., 2006). Geochemical analysis of subsequent ash discoveries across India showed that they all belonged to the YTT (Acharyya and Basu, 1993; Shane et al., 1995; Westgate et al., 1998). The purity of the ash and its widespread distribution across India show that a layer of ash sufficiently thick to preclude contamination with the underlying soils covered much of the sub-continent to a maximum depth of 10–15 cm, as in the adjacent Bay of Bengal marine cores (Ninkovich et al., 1978a; Acharyya and Basu, 1993; Gasparotto et al., 2000). Erosion of the unconsolidated ash mantle deposited across the landscape would have been a rapid process leading to choking of low order stream channels within a few years, just as on Mount St Helens after the May 1980 eruption (Collins and Dunne, 1986).

3. Stable carbon and oxygen isotope analysis of soil carbonates in central India

3.1. Location of sites

We have sampled palaeosol carbonates above and beneath Toba ash outcrops at three locations with very fine-grained (<67 μm) stratified Toba ash along a NE–SW transect spanning 400 km (Fig. 1), including two on either bank of the Son River (Khunteli and Rehi) and one near Hirapur village on the Biranj River (a tributary of the Narmada River) (Fig. 1). The two Son Valley sites (Rehi and Khunteli) are exposed as Late Pleistocene cliff sections overlooking the modern river (Williams and Royce, 1982; Acharyya and Basu, 1993; Williams et al., 2006). The third site is exposed in a terrace near Hirapur village, located 4 km north of the Narmada River, on the Biranj River, tributary to the Narmada (Acharyya and Basu, 1993; Mukhopadhyay and Ramachandra, 1997). Section 3.4 provides detailed descriptions of the stratigraphic sections.

At Hirapur, the Toba ash lies conformably within the 12 m thick Baneta Formation comprising fine-grained silts and silty/sandy loams

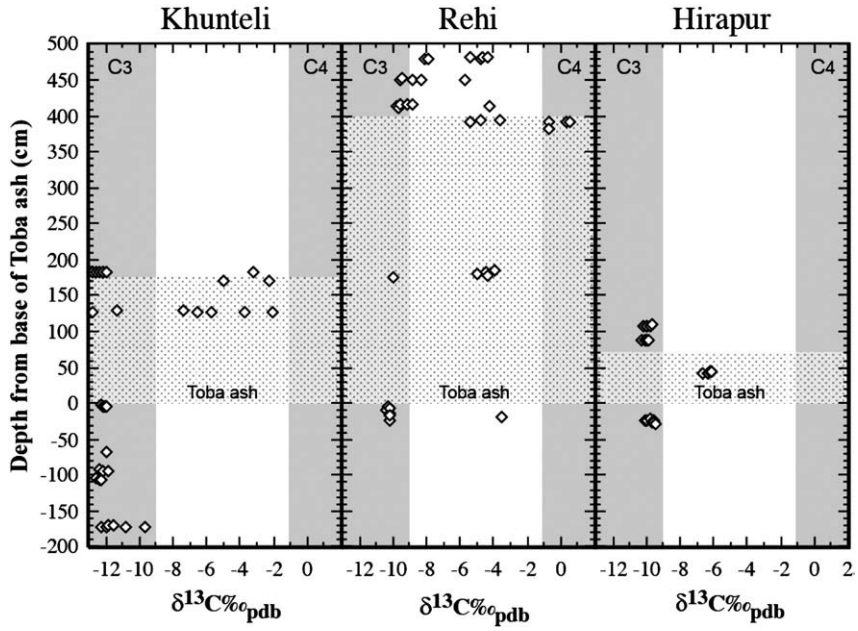

Fig. 2. $\partial^{13}C$ values of pedogenic carbonates versus depth above/below the base of the Toba ash in the Khunteli, Rehi and Hirapur sections. The stippled section shows the position and thickness of the Toba ash. The shaded margins show the ranges of $\partial^{13}C$ values of pedogenic carbonates formed in pure C_3 and pure C_4 floral habitats.

(Mukhopadhyay and Ramachandra 1997). Pedogenic carbonates occur below and above the 125 cm thick ash and within the pedogenically altered upper 55 cm of the ash.

3.2. Methods of analysis

Carbonate samples were prepared for analysis at the Environmental Isotope Paleobiogeochemistry Laboratory, Department of Anthropology, University of Illinois, Urbana. Nodules ranged from 13 to 50 mm in maximum length. Rootcasts selected for analysis were >8 mm diameter. All nodules and rootcasts had micritic (fine-grained) textures with no visible crystallinity. Samples were extracted from the cores of freshly fractured specimens using a mini-drill with a diamond burr. To prevent thermal decomposition the drill speed was set to its lowest setting, and lowered further by reducing the power to ~90 V with a voltage regulator.

Samples of carbonate and Toba ash weighing on average 36 ± 14 mg (mean ± 1 standard deviation) were heated to 380–400 °C under vacuum for 3 h to reduce organic matter, and to remove adsorbed water and weakly bound clay hydroxyls. Weight loss from heating (Table 2) is usually greater for samples with lower carbonate contents. CO_2 for carbon and oxygen isotope analysis was generated by reaction of carbonate samples with 100% phosphoric acid at 70 °C in a Kiel III automated carbonate reaction–cryogenic distillation device interfaced with a Finnegan MAT 252 isotope ratio mass spectrometer at the Illinois State Geological Survey. Samples for reaction weighed 30–110 μg (mean and standard deviation: 59 ± 14 μg). Two pure Toba ash samples taken from the lower, pedogenically unaltered parts of the

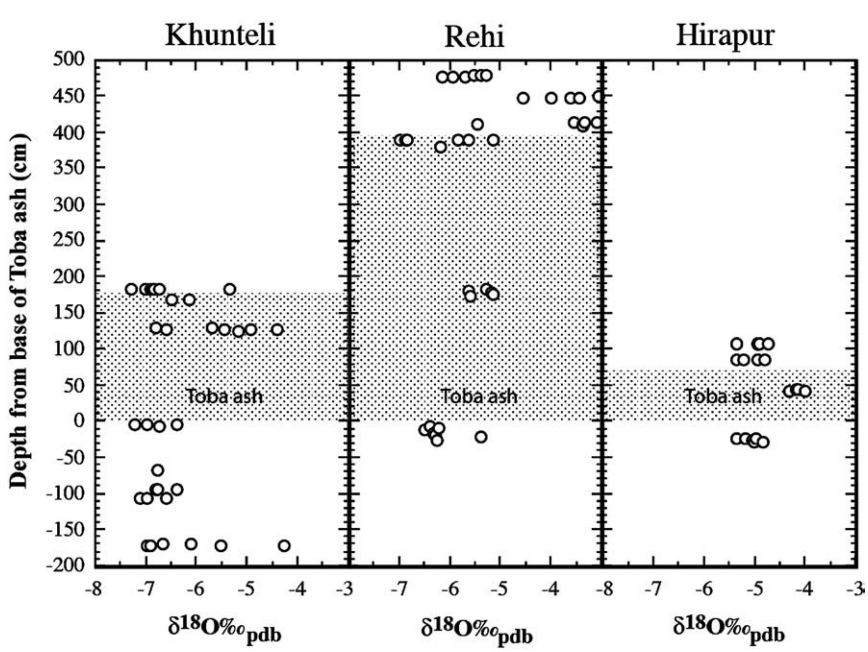

Fig. 3. Oxygen isotope ratios of pedogenic carbonates versus depth above/below the base of the Toba ash in the Khunteli, Rehi and Hirapur sections.

Khunteli and Rehi sections, weighing 1094 and 542 μg, respectively, were also heated in vacuo and reacted; they produced undetectable amounts of CO_2. (Table 2) Yields of carbonate carbon are calculated based on the manometer pressure of purified CO_2 in the Kiel device, calibrated by a range of weights of calcite isotopic standard reference materials NBS-18 and NBS-19, assuming the mineral phase analysed is calcite ($CaCO_3$). Pure calcite is ~12% C by weight.

Isotope ratios are expressed using the δ notation as permil (‰, or parts per thousand) difference from those of the Pee Dee Belemnite standard, calculated as:

$$\delta‰ = (R_{sample} / R_{standard}) - 1 \times 1000$$

where R is $^{13}C/^{12}C$ or $^{18}O/^{16}O$. Precision and replicability of NBS 18 and NBS 19 standards for $\delta^{13}C$ is 0.1 ± 0.09‰, and for $\delta^{18}O$ is 0.16 ± 0.14‰ with the Kiel device on this mass spectrometer.

3.3. Use of stable carbon isotopes to infer vegetation type

The carbon isotope composition of carbonate nodules and rootcasts formed within sediments and soils interstratified with the YTT can provide direct evidence for the impact of the Toba eruption on tropical environments because it provides a quantitative estimate of the proportions of trees to grasses (Cerling, 1984; Ambrose et al., 2007). Trees, shrubs, most dicotyledonous herbs and shade-tolerant grasses use the C_3 photosynthetic pathway and have low $\delta^{13}C$ values, averaging ca. −26‰ (Smith and Epstein, 1971). Tropical grasses that are adapted to strong sunlight, high temperatures, aridity and low atmospheric CO_2 concentrations use C_4 photosynthesis and have higher $\delta^{13}C$ values, averaging ~−12‰ (Ehleringer et al., 1997). Heat, water stress and/or reduced atmospheric CO_2 concentrations favour the growth of plants with the C_4 photosynthetic pathway (Ehleringer et al., 1997; Collatz et al., 1998). Some C_4 species have evolved cold-tolerant physiological adaptations (Wang et al., 2008), which may, along with low CO_2 concentrations (Ward et al., 2008), account for their abundance in low latitude glacial paleoenvironments.

Soil organic matter derived from C_4 plants has high $\delta^{13}C$ values, averaging −12‰, while that from C_3 plants averages −26‰ (Ambrose and Sikes, 1991). The carbon isotope ratio of pedogenic carbonate reflects that of the floral biomass, with an enrichment of 14–17‰ (Cerling, 1984). Pedogenic carbonates formed under forests thus have $\delta^{13}C$ values of −12‰ to −9‰, while $\delta^{13}C$ values of those formed under C_4 grasslands range from −1‰ to +2‰. The precision and accuracy of estimates of proportions of C_3 and C_4 biomass vary due to time averaging of biomass isotopic composition during carbonate formation. Variation can be assessed by analysis of several carbonate nodules and rhizoliths at each level sampled. The minimum estimate of the range of variation is no less than the range of isotope ratios of nodules analysed.

Pedogenic carbonate $\delta^{18}O$ values are a complex function of rainwater source isotopic composition, distance from evaporative source, rainfall amount, temperature, humidity, altitude and latitude. All else being equal, carbonate $\delta^{18}O$ value are highest in hot, arid habitats and at low latitudes and altitudes (Cerling, 1984).

3.4. Description of the Khunteli, Rehi and Hirapur stratigraphic sections

At Khunteli (Fig. 1) the Toba ash appears to be an avulsion deposit that occupies a channel fill eroded into the sands and clays of the Late Pleistocene Khunteli Formation (Williams et al., 2006). In the excavated section at Khunteli, the upper 175 cm of the sands beneath the ash consist of alternating medium sand beds 27–56 cm thick and brown silty clay and clayey silt bands up to 9 cm thick, containing pedogenic carbonate concretions and rootcasts. The ash is a discontinuous bed of volcanic ash up to 1.83 m thick. The upper 70 cm of the ash is reworked, and grades into a massive fine-grained silt palaeosol with pedogenic carbonates. Vertical cracks filled with carbonate run through the excavated section. Sediments above the excavated section comprise at least 4 m of cross-bedded and planar-bedded medium and coarse sands and fine gravels and an upper unit of carbonate cemented gravels.

The 30 m thick section on the left (north) bank of the River Son near its confluence with the River Rehi is a lateral variant of Khunteli Formation, and consists of a basal unit up to 8 m thick of brown medium sand capped by a laterally discontinuous unit of volcanic ash up to 4 m thick (Williams and Royce, 1982). In Section 1 of the Son–Rehi YTT outcrop, the upper 20 cm of the brown sands are coarse and laminated, and contain sparse small carbonate nodules comprising cemented coarse sand. In the 5 m deep excavated section (Section 2), the brown sand is capped by 25 cm of clayey silt (mudstone) with small carbonate rootcasts. In Section 1 this mudstone is thinner. Small diapiric intrusions of this mudstone into the overlying pure Toba ash suggest the ash was deposited over a soft wet mud. In Section 2, the basal 1.1 m of the ash is pure, but from 1.1 to 3.45 m it grades into an ashy silt–loam with carbonate nodules and rootcasts. The reworked ash is completely cemented with carbonate from 3.45 to 3.83 cm above the base of the ash. 1.8 m of dark brown well-developed vertic palaeosols with abundant carbonate nodules conformably overlie the cemented ash.

The Toba ash in the 12 m Hirapur section lies within the fine-grained silts and silty/sandy loams of the Baneta Formation. In Fig. 2 of

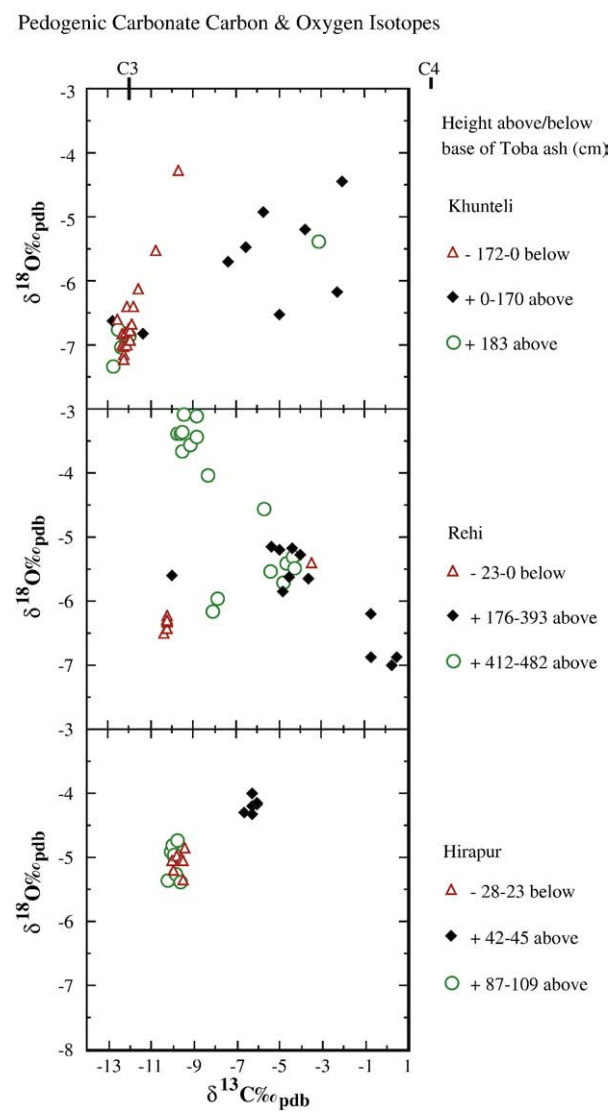

Fig. 4. Bivariate plot of carbon and oxygen isotope ratios of pedogenic carbonates in the Khunteli, Rehi and Hirapur sections. Samples below the Toba ash: red triangles; within the ash: black diamonds; above the ash: green circles.

the report by Mukhopadhyay and Ramachandra (1997) describing this locality, the Hirapur section label was transposed with that for Guruwara, which is located about 70 km east on the Narmada River. Our main excavated section (Trench 2) comprises 3.2 m of brown sandy clay loam with carbonate nodules in the top 30 cm. The basal 70 cm of the overlying ash is relatively pure, while the upper 55 cm is reworked, with heterogeneous patches of pure ash and darker clay loam, and carbonate rootcasts and nodules. A dark brown sandy palaeosol conformably overlies the reworked ash. Clayey alluvium/colluvium with historic artifacts unconformably overlies this palaeosol. In Trench 1, located ~12 m from Trench 2, the primary ash bed is 25 cm thick, overlain by 22 cm of reworked ash. Carbonate nodules within the reworked ash formed from plants growing on the overlying brown clayey loam palaeosol.

3.5. Results of stable carbon isotope analysis

We have analysed the carbon and oxygen isotopic composition of 92 pedogenic carbonate nodules and rootcasts from four excavated sections. Five additional carbonate samples listed in Table 1 are considered non-pedogenic. The isotopic composition of carbonates formed within the first soils formed on Toba ash parent material reflects that of the plant community.

Minimum $\delta^{13}C$ and $\delta^{18}O$ values for the localities sampled (Table 2; Figs. 2–4) increase from NE to SW, possibly reflecting a steeper gradient of higher average annual temperature and lower rainfall than prevails today. Khunteli, with the lowest average $\delta^{13}C$ values beneath the ash (−11.9‰) shows that immediately before the Toba eruption, central India may have supported a relatively dense closed forest on the east; progressively higher values for Rehi (−10.3‰) and Hirapur (−9.7‰) suggest more open forest to closed woodland toward the west. The increase in $\delta^{18}O$ values from east to west is paralleled by an equivalent increase in those of modern rainfall and groundwater, reflecting a Rayleigh distillation process of rainout from prevailing westerly air masses carried from the Indian Ocean (Gupta et al., 2005; Gupta and Deshpande, 2005).

Low $\delta^{13}C$ values (−12.6 to −9.5‰) for 30 of 31 nodules beneath the Toba ash at all sites show that the ash fell on nearly pure C_3 habitats that were probably forested (Fig. 2). High $\delta^{13}C$ values (−7.4‰ to +0.5‰) for 24 of 27 nodules within the upper parts of the ash show that the first post-eruption soils supported floras that were dominated by C_4 grassland to wooded grassland habitats. Extremely high $\delta^{13}C$ values (−0.7‰ to +0.5‰) in the level 3 calcrete horizon at Rehi indicate nearly pure C_4 grassland persisted for a long time in this part of the Son Valley. Very low $\delta^{13}C$ values above the ash indicate C_3 forest habitats eventually returned to Khunteli and

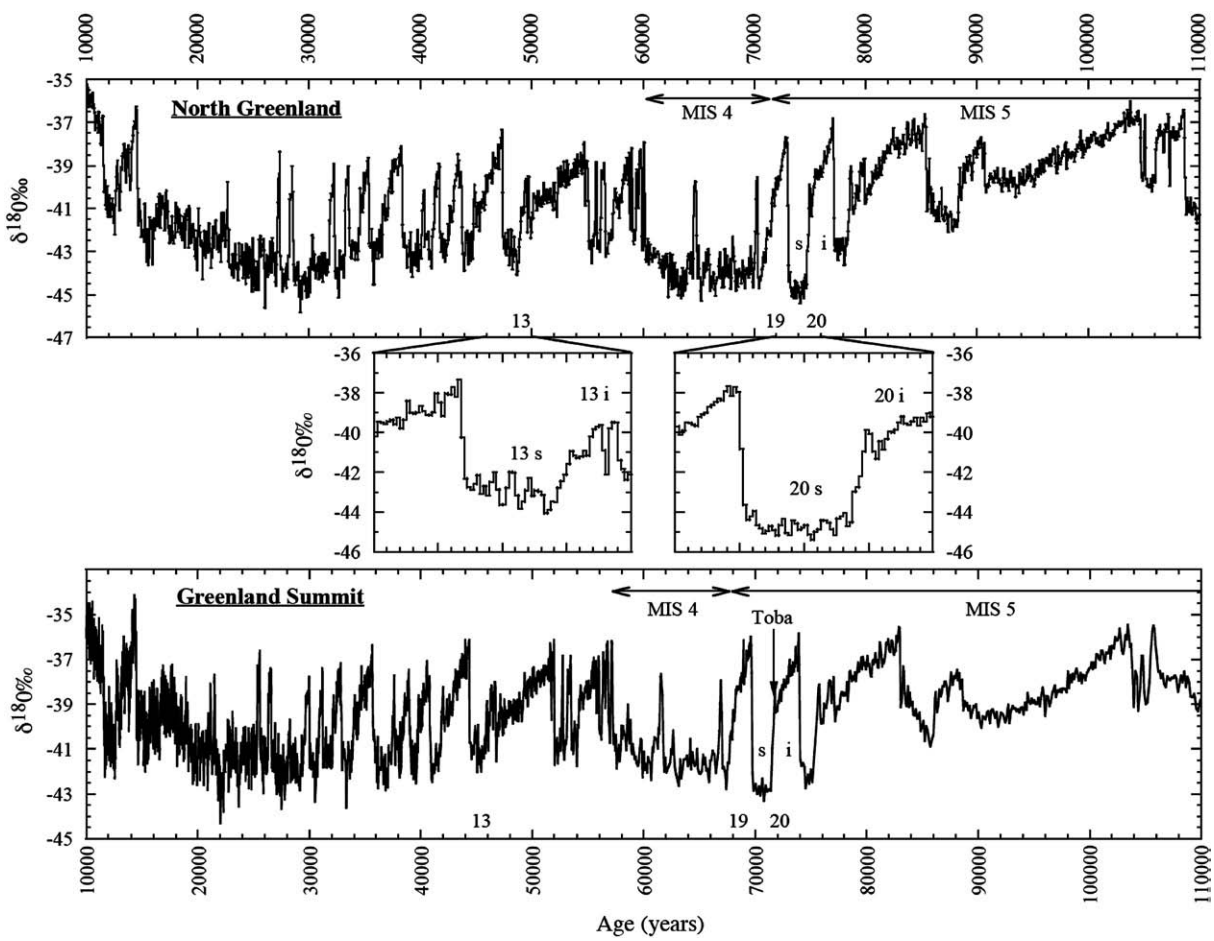

Fig. 5. North Greenland and Greenland Summit ice core oxygen isotope ratios from 10 to 110 ka, showing Dansgaard–Oeschger cycles 19 and 20, and the boundary between Marine Isotope Stage (MIS) 4 (early last glacial maximum) and MIS 5 (last interglacial). The position of the volcanic sulfate peak attributed to Toba in the Summit GISP2 core (Zielinski et al., 1996) is indicated with an arrow, and the stadial (cold) and interstadial (warm) halves of D–O 20 are indicated by s and i, respectively. The chronological position of the termination of the D–O 20 interstadial in the North Greenland core (NGRIP, 2004) is concordant with radiogenic argon dates for the Toba eruption (Chesner et al., 1991), while that for the Summit cores is approximately 2000 years younger (Dansgaard et al., 1993; Johnsen et al., 2001). Recalibration and correlation of the Greenland ice cores with the U-series dated Hulu Cave speleothem (Weninger and Jöris, 2008) is concordant with the age of the North Greenland core and the argon isotope age of the Toba eruption. The inset figures compare two 4000-year segments of the North Greenland core (D–O 13 and 20, 46–50 and 72–76 ka, respectively) in order to emphasize the extreme cold, low temperature variance and long duration of the D–O 20 stadial. These data show that the stadial component of D–O 20 was the longest (1500–1800 years) period with the consistently lowest ice $\delta^{18}O$ values of both ice core records.

Hirapur, while low to intermediate values indicate that a mosaic of forest to wooded grassland habitats eventually predominated at Rehi.

Although low temperatures that followed the eruption during D–O stadial 20 are considered unfavourable for C_4 plants, they have a competitive advantage over C_3 plants when atmospheric CO_2 concentrations are low (Ehleringer et al. 1997; Ward et al., 2008), and some C_4 species are remarkably cold-tolerant (Wang et al., 2008). Air CO_2 concentrations in Greenland ice dropped rapidly during cold stadials (Smith et al. 1997), so C_4 photosynthesis would have remained advantageous following the Toba eruption during the 1800 year stadial portion of D–O 20.

The Toba ash was therefore deposited on a landscape covered by mainly C_3 plant communities (probably forests) that were then replaced by mainly C_4 grasslands or wooded grasslands. However, the time needed for these soils to develop and for the carbonate concretions to form is not known and could range from 10^2 to 10^3 years. We cannot accurately estimate how much time elapsed before the post-eruption C_4-dominated grassland environment was replaced by forest and woodland because terrestrial sedimentation and soil formation rates are highly variable, and applicable chronometric methods have relatively low precision and accuracy. However, at Rehi the soil that formed under nearly pure C_4 grassland on reworked Toba ash is over 2.1 m thick. The top 30 cm of this soil is completely cemented with pedogenic carbonate, indicating that this grassland may have persisted for more than a millennium (Machette, 1985). This millennial-scale estimate is consistent with the ice core record of low atmospheric CO_2 (Smith et al., 1997) and extremely cold temperatures during the ~1800 years' duration of D–O stadial 20 (Fig. 5).

4. Analysis of terrestrial pollen in marine core S0188-342KL, Bay of Bengal

4.1. Selection of samples for pollen analysis

In order to improve our estimate of the duration and geographical range of this period of deforestation in central India, we decided to seek independent evidence from fossil pollen in a marine sediment core in which Toba ash is well preserved and sedimentation rates can be more accurately estimated. Marine core S0188-342KL, located in the northern Bay of Bengal, came from 1256 m water depth at 19°58.41′N and 90°02.03′E (Fig. 1). The sediment consists of greenish-grey foraminifera-bearing silty clay and the Toba ash is at 598 cm depth within the core. The core section studied covers the period from ~5500 years before to ~3500 years after the Toba eruption, deduced (a) from the position of the ash layer on the $\delta^{18}O$ isotopic curve of G. ruber and (b) from the major element composition of glass shards analysed. The sedimentation rate above the ash is estimated to be 6.1 cm/kyr. Samples selected for pollen analysis from the marine core had to fulfil two criteria. (a) We needed close sampling above and below the YTT in order to pick up any abrupt changes in vegetation cover. (b) We needed samples covering the stage 5/4 transition at lower resolution to identify any gradual changes in vegetation cover that may relate to this transition rather than the Toba eruption. The interpretation we present below deals only with sudden changes around the YTT in the pollen record. Any gradual changes have been ignored as they are most likely part of the stage 5/4 transition.

4.2. Methods used in the pollen analysis

Samples from core S0188-342KL were processed following the procedures outlined in van der Kaars et al. (2000). Approximately 3.8–4.3 ml of sediment was suspended in about 40 ml of tetra-sodium-pyrophosphate (±10%) and subsequently sieved over 210 and 7 micron meshes, followed by hydrochloric acid (10%) treatment and heavy liquid separation (sodium–polytungstate, SG 2.0, 20 min at 2000 rpm). Slides were mounted in glycerol and sealed with paraffin wax. A known amount of *Lycopodium* marker spores was added to each sample before chemical treatment in order to establish palynomorph concentrations.

All slides were counted along evenly spaced transects until a minimum count of 275 dryland pollen grains was reached for core S0188-342KL. All percentage values were calculated on the total dryland pollen sum. Pollen concentration values are presented as the total dryland pollen grains per ml of sediment. The differences in the pollen counting sums used are tuned to the vegetation from which the pollen signal is derived. The vegetation types represented in core SO188-342KL are quite varied and therefore the pollen sum was made up of all dryland pollen (trees, shrubs and herbs).

4.3. Age model developed for the marine core

Fig. 6 shows the age model that we have developed for marine core SO188- 342KL. The timescale was constructed by correlating variations in the *a** values (determined from colour reflectance) in core SO188-342KL (data shown in red) and SO93-126KL (blue) around the Younger Toba volcanic ash layers (marked by the green vertical line at 73 ka) which are situated at 665 cm core depth in 126KL and at 598 cm in 342KL (c). Core 126KL was recovered in 1994, twelve years earlier than core 342KL which is from the same location (19°58.40′N, 90°02.03′E, water depth 1253 m), but which had been so intensively sampled that it had too little material left for pollen analysis. This difference in storage period has caused stronger oxidation of the sediments in 126KL leading to more reddish colours. For better comparison we thus systematically corrected the *a** values for 126KL by −0.4. The age model for core 126KL (Kudrass et al., 2001) in turn is based on radiocarbon dates between the core top and 40,000 calendar years (40 ka). Variations in the oxygen isotope composition of the planktonic foraminifera *Globigerinoides ruber* (white) from 126KL (b) closely covary with shifts in the oxygen isotope composition of the Greenland Ice Sheet Project 2 (GISP2) ice (a) in the radiocarbon-dated

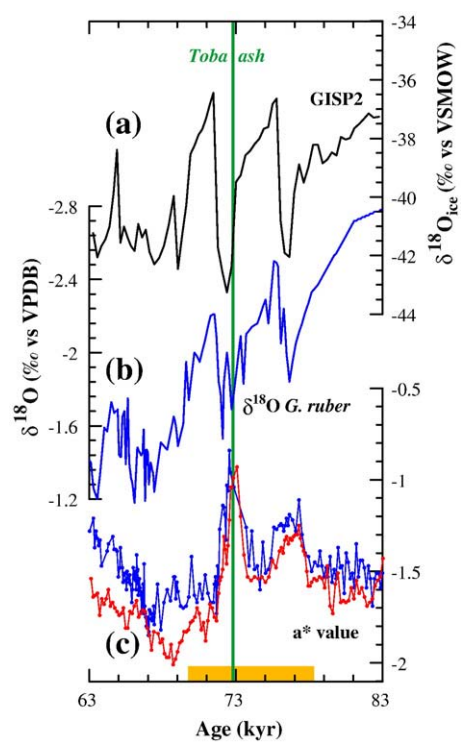

Fig. 6. Age model developed for marine core SO188-342KL (explained in text). From top to bottom: Greenland Ice Sheet Project 2 (GISP2) $\partial^{18}O$ values of ice; $\partial^{18}O$ values for the planktonic foraminifera *Globigerinoides ruber* (white); a* values (more negative values indicate green while more positive values indicate red) determined from colour reflectance in core SO93-126KL (shown in blue) and core 342KL (shown in red). The green vertical line denotes the isochronous time marker of the Toba ash, here estimated at 73 ka. The yellow bar at the bottom of the figure denotes the range of samples for pollen grain counts.

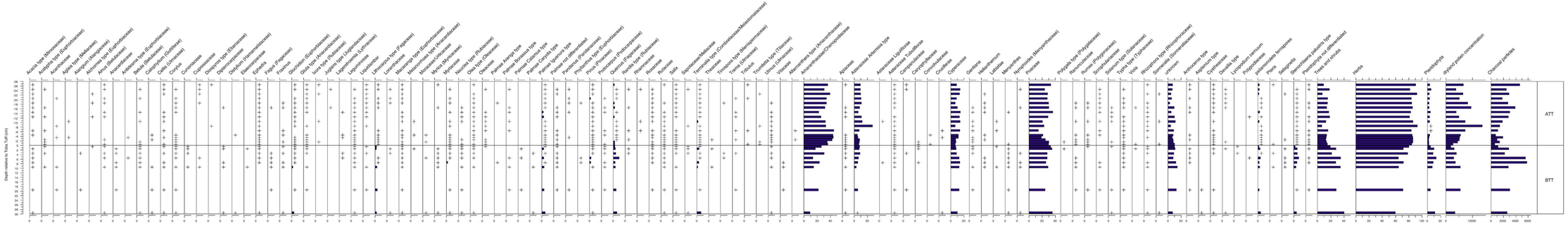

Fig. 7. Detailed pollen diagram of part of marine core 50188-342Kl. from the Bay of Bengal (19°58.41′N; 90°02.03′E) showing changes in pollen spectra after the Toba eruption.

section of 126KL. Therefore the planktonic d^{18}O curve was used to adjust the older part (>40 ka) of 126KL to the GISP2 timescale (Grootes et al., 1993; Meese et al., 1997). We adjusted the age of the GISP timescale in order to place the end of interstadial 20 at 73 ka, coinciding with the age of the Toba eruption as determined by Ninkovich et al. (1978b) and Chesner et al. (1991).

The 73 ka age for the Toba eruption used in our model is based on the K–Ar age of 73.5 ± 3 ka obtained for the eruption by Ninkovich et al. (1978b) and the single-grain laser-fusion ^{40}Ar/^{39}Ar age of 73 ± 4 obtained by Chesner et al., 1991). This agrees with the age model for the North Greenland core, and the U-series dates for the Hulu Cave speleothem (Weninger and Jöris, 2008). We are aware that the error terms associated with the K/Ar ages obtained for the Toba eruption could amount to ± 4 ka. However, we note *that establishing an exact age for the ash is not essential for our purposes, since our concern is to determine the environmental changes that immediately followed the eruption*. The sedimentation rates obtained using our model are broadly correct and can be fine-tuned once the pre- and post-Toba eruptive rocks have been re-dated. Regardless of the absolute age, the YTT provides an isochronous marker for correlating the cores to each other, and to the terrestrial sections described above. Moreover, the ice core evidence for volcanic sulfate from the Toba eruption (Zielinski et al., 1996) unequivocally ties these tropical marine and terrestrial sequences to the global climatic record.

4.4. Pollen diagram

The pollen assemblages are dominated by herbaceous taxa, with substantial numbers of Amaranthaceae/Chenopodiaceae, Artemisia, Cyperaceae and Poaceae, with minor representation of arboreal taxa indicating the presence of vegetation largely consisting of herblands and open woodlands (Figs. 7 and 8). A significant reduction in tree and shrub numbers and Pteridophyta after the Toba eruption suggests drier conditions. However, the marked reduction in *Stenochlaena palustris*, a fern mostly restricted to wet environments in the lowland tropics from sea level to 300 m elevation may also point to cooler conditions. Overall, the distinct change to more open vegetation cover and reduced representation of ferns, particularly in the first 5–7 cm above the Toba ash, would suggest significantly drier conditions in this region for at least one thousand years after the Toba eruption.

4.5. Direct and indirect impacts of the Toba super-eruption upon plant cover

Two questions relating to the interpretation of the pollen preserved in the Bay of Bengal marine core concern the direct impact of the eruption upon the plant cover (explosive blast; fires) and the degree to which the pollen in marine cores is truly representative of the terrestrial record.

The 1850 BP eruption from Taupo in New Zealand offers a useful insight into both questions (Wilmhurst and McGlone, 1996; Wilmhurst et al., 1999). This eruption covered 30 000 km^2 of the central North Island with ash and roughly 20 000 km^2 with ignimbrite, the latter destroying all forests beneath the ash flow deposits. The pollen record shows that forests located up to 170 km east of the Taupo eruption suffered some degree of damage, but re-vegetation was complete within 200 years of the eruption, with post-eruption forests similar to those growing before the eruption. The impacts on plant cover of smaller eruptions from Taupo were less evident in the marine record, which showed some slight time lags between the instantaneous deposition of volcanic ash and the slower arrival of sediment brought in by rivers from the source area, but even major eruptions caused but brief increases of a few centuries' duration in the terrigenous sediment influx from fluvial redistribution of volcanic deposits (Carter et al., 2002). We may conclude from the well-documented Taupo record that the Toba super-eruption probably had little long-term effect on deep sea sedimentation rates in the core we have analysed. There may have been some slight time lags in the arrival of pollen carried in by rivers after the initial eruption. Given the distance of the marine core site from Toba volcano (~2200 km), it is extremely improbable that any of the post-eruption vegetation changes we have identified reflect the immediate and direct effects of the eruption upon

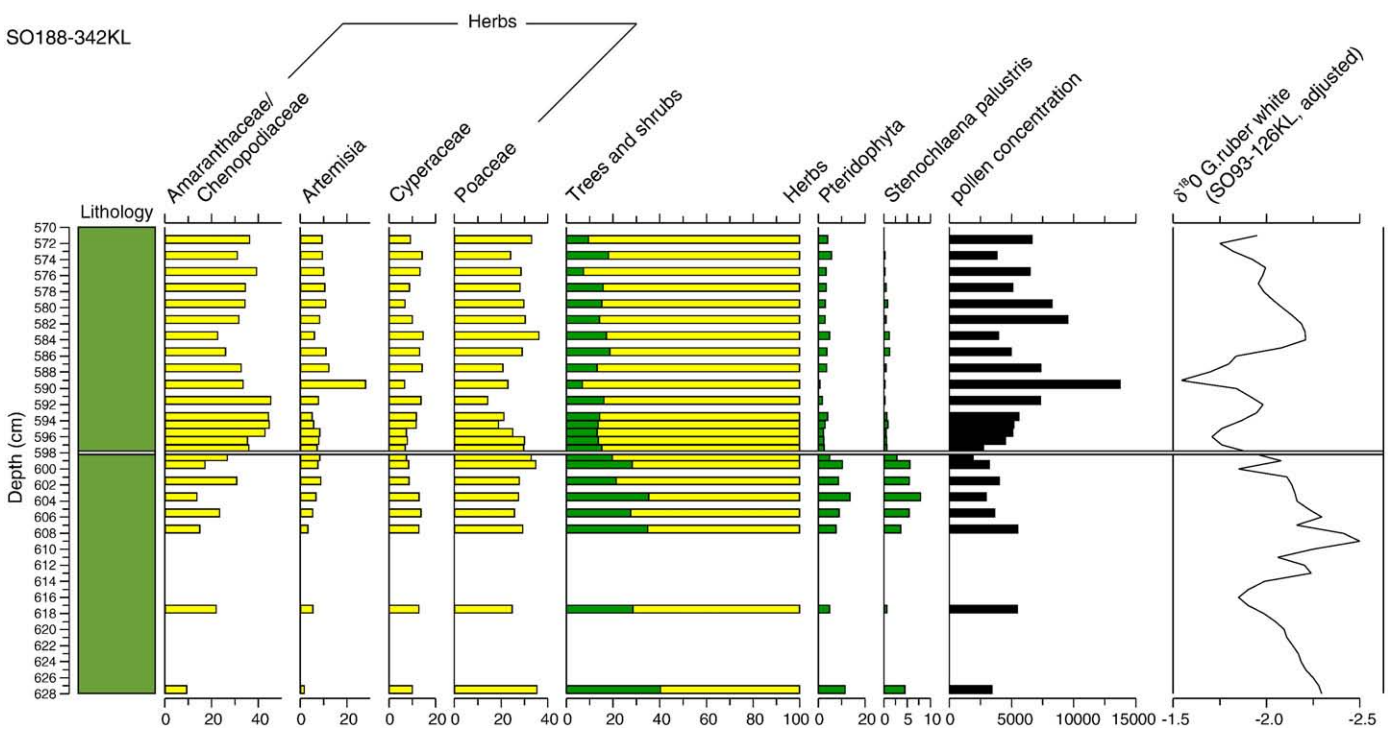

Fig. 8. Simplified pollen diagram of part of marine core S0188-342KL from the Bay of Bengal (19°58.41′N; 90°02.03′E) showing changes in pollen spectra after the Toba eruption. Changes in δ^{18}O values for the planktonic foraminifera *Globigerinoides ruber* (white) are shown alongside the pollen curves to facilitate comparison with Fig. 6.

the landscape. In any event, these effects are unlikely to have persisted for more than a very few centuries in this tropical environment. The longer-term effects we consider more likely to reflect changes in local and regional climate resulting from the eruption.

5. Discussion

5.1. Possible climatic impact of the Toba super-eruption

The Toba eruption marks the onset of the coldest two millennia of the Greenland ice cores (Dansgaard et al., 1993; Zielinski et al., 1996; Lang et al., 1999; North Greenland Ice Project Members, 2004). It is likely that the formation of the fossil soil carbonates in the Rehi section and the first 5–10 cm of the marine core above the Toba ash span the duration of this stadial interval. Small numbers of Middle Palaeolithic artifacts from gravels and sands stratified below and above a thick bed of ash in south India have been interpreted as demonstrating insignificant impacts of Toba on terrestrial environments and human adaptations in India (Petraglia et al., 2007). Our results challenge this conclusion because they show that the Toba eruption led to prolonged drought and deforestation in India, probably lasting for 1000–2000 years. Cooling arising from the Toba super-eruption is considered responsible for the extreme cold of ice core stadial 20 (Zielinski et al., 1996) and is supported by our work. The precise magnitude and duration of the Toba-induced cooling in other regions of the world is still not well known, because their environmental records are not stratified with clear markers of the 73 ka Toba eruption. However, cores from three large, deep lakes in tropical Africa (Lakes Malawi, Tanganyika and Bosumtwi) have unusual depositional events at ~73 ka, reflecting apparently synchronous abrupt drops in lake levels (Scholz et al., 2007). This is consistent with a severe global environmental impact for the Toba-induced cooling.

A major uncertainty concerns the physical processes responsible for such a prolonged duration. Rousseau and Kukla (2000) noted rapid monsoon retreat in China at the S1/L1 boundary of the long loess-palaeosol sequence of the Loess Plateau, and suggested that the most likely cause was sudden rearrangement of the oceanic conveyor belt, perhaps triggered by the Toba eruption. The cooling effects of historic eruptions are known to involve the generation of highly reflective low-level clouds produced by sulfate aerosols and of dust veils scattering solar radiation (Rampino and Self, 1982; Rampino et al., 1985; Sadler and Grattan, 1999) and vary spatially over time (Kelly et al., 1996). However, such cooling is short-lived, lasting only several years, after which the aerosols and dust particles are scavenged by falling rain. The cooling generated by the Toba sulfates (Zielinski et al., 1996) may have been accentuated in high latitudes through positive feedback effects related to increased albedo from persistent snow cover at high latitudes (Rampino and Self, 1993; Zielinski et al., 1996; Kelly et al., 1996; Jones et al., 2005).

The Greenland GRIP Summit ice core record shows a repetitive sequence of cold (stadial) and warm (interstadial) cycles (see Williams et al., 1998, for a detailed discussion), each ~1–3 ka in duration. The cycle analysed by Lang et al. (1999) shows a very rapid 16 °C change in temperature at about the time of the Toba eruption, but in the absence of direct geochemical evidence we cannot be certain that it reflects the climatic impact of the Toba eruption. Millennial-scale variation in $\delta^{18}O$ of atmospheric O_2 in the North Greenland ice core is correlated with evaporative enrichment in transpired plant leaf water, and an abrupt increase in percentages of semi-desert plant biomass in Mediterranean Sea core ODP 976 at ~74 ka (Genty et al., 2005; Landais et al., 2007). If the Toba eruption did indeed coincide with the onset of the very cold event just after interstadial 20, as seems probable (Zielinski et al., 1996), then the Toba eruption may have provided the catalyst for the prolonged cooling and drying that followed. In any event, the impact on prehistoric human societies would have been profound, as indicated by the genetic evidence (Harpending et al., 1993; Ambrose, 1998; Forster, 2004).

5.2. Implications for prehistoric human migrations

If global primary productivity declined catastrophically for nearly two millennia following the Toba eruption then it may have been responsible for the late Pleistocene population bottlenecks reflected in the genetic structure of living human (Harpending et al., 1993; Mountain and Cavalli-Sforza, 1997; Watson et al., 1997; Ke et al., 2001; Forster, 2004), eastern African chimpanzee (Goldberg, 1996), Bornean orangutan (Steiper, 2006), central Indian macaque (Hernandez et al., 2007) and all tiger (Luo et al., 2004) populations, and the separation of the nuclear gene pools of eastern and western lowland gorillas (Thalmann et al., 2007). Molecular genetic dating indicates that all of these species recovered from very low population sizes during the early last glacial, ~70–55 ka.

The Toba-induced cooling may have also forced African human populations to develop new strategies for survival. The final stages of the transition to modern human behaviour, which included the development of strategic risk-minimizing social information and materials long distance exchange networks, appeared in the archaeological record in East Africa soon after this eruption (Ambrose, 2002, 2006). This new cooperative social strategy may have been crucial for human survival in degraded environments after the eruption, and may have also facilitated the dispersal of modern humans from Africa and replacement of archaic human populations outside of Africa during the last ice age (Ambrose, 2002; Mellars, 2006; Beyin, 2006).

6. Conclusions

The Toba ash provides an unambiguous isochronous stratigraphic marker for correlation of terrestrial (Westgate et al., 1998), marine (Song et al., 2000) and ice core (Dansgaard et al., 1993; Lang et al., 1999; North Greenland Ice Project Members, 2004) environmental records. Our new carbon isotope evidence from fossil soils found immediately beneath and above the Toba ash in central India demonstrates a major isochronous change in vegetation from forest before the eruption to open woodland or grassland thereafter. Terrestrial pollen spectra from a marine core collected from the Bay of Bengal support the terrestrial isotopic evidence indicating initially cooler temperatures followed by decreased tree cover and prolonged drought for at least a millennium following the Toba eruption. These terrestrial and marine archives of climatic change following the Toba super-eruption provide support for the hypothesis that severe environmental degradation could have been responsible for large mammal extinctions in southeast Asia and genetic bottlenecks in humans and other species that occurred in Africa and southeast Asia at this time.

Acknowledgements

We thank the Australian Research Council (MAJW), the National Science Foundation (SHA) and the University of Allahabad (UC, JP) for logistical support, Grant McTainsh for the particle size analysis of the Toba ash from the Son–Rehi section in India, and Brad Pillans, Chris Turney and two anonymous referees for constructive criticism of earlier drafts.

Author Contributions. MAJW designed the research program. MAJW, SHA, PC UC and JP collected samples in India. SHA performed the isotopic analysis of carbonates. CR collected marine core S0188-342KL. SvdK analysed the pollen from the marine core. MAJW, SHA, SvdK, CR and PC wrote the paper. All authors discussed the results and commented on the manuscript.

References

Acharyya, S.K., Basu, P.K., 1993. Toba ash on the Indian subcontinent and its implications for correlation of Late Pleistocene alluvium. Quaternary Research 40, 10–19.

Ambrose, S.H., 1998. Late Pleistocene human population bottlenecks, volcanic winter, and differentiation of modern humans. Journal of Human Evolution 34, 623–651.

Ambrose, S. H., 2002. Small things remembered: origins of early microlithic industries in sub-Saharan Africa. In: Elston, R., Kuhn, S. (Eds), Thinking Small: Global Perspectives on Microlithization. Archaeological Papers of the American Anthropological Association, No. 12, Washington, D.C., pp. 9-29.

Ambrose, S.H., 2003. Did the super-eruption of Toba cause a human bottleneck? Reply to Gathorne-Hardy and Harcourt-Smith. Journal of Human Evolution 45, 231–237.

Ambrose, S.H., 2006. Howiesons Poort lithic raw material procurement patterns and the evolution of modern human behavior: a response to Minichillo. Journal of Human Evolution 50, 365–369.

Ambrose, S.H., Sikes, N., 1991. Soil carbon isotope evidence for Holocene habitat change in the Kenya Rift Valley. Science 253, 1402–1405.

Ambrose, S.H., Williams, M.A.J., Chattopadhyaya, U., Pal, J., Chauhan, P., 2007. Environmental impact of the 73 ka Toba eruption reflected by paleosol carbonate carbon isotope ratios in central India. Quaternary International 167–168, 8.

Bekki, S., Pyle, J.A., Zhong, W., Toumi, R., Haigh, J.D., Pyle, D.M., 1996. The role of microphysical and chemical processes in prolonging the climate forcing of the Toba eruption. Geophysical Research Letters 23, 2669–2672.

Beyin, A., 2006. The Bab al Mandab vs the Nile-Levant: an appraisal of the two dispersal routes for early modern humans out of Africa. African Archaeological Review 23, 5–30.

Bowler, J.M., Johnston, H., Olley, J.M., Prescott, J.R., Roberts, R.G., Shawcross, W., Spooner, N.A., 2003. New ages for human occupation and climatic change at Lake Mungo, Australia. Nature 421, 837–840.

Bühring, C., Sarnthein, M., Leg 184 Shipboard Scientific Party, 2000. Toba ash layers in the South China Sea: evidence of contrasting wind directions during eruption ca. 74 ka. Geology 28, 275–278.

Carter, L., Manighetti, B., Elliot, M., Trustrum, N., Gomez, B., 2002. Sea level and circulation effects on the sediment flux to the deep ocean over the past 15 ka off eastern New Zealand. Global and Planetary Change 33, 339–355.

Cerling, T.E., 1984. The stable isotopic composition of modern soil carbonate and its relationship to climate. Earth and Planetary Science Letters 71, 229–240.

Chesner, C.A., Rose, W.I., Deino, A., Drake, R., Westgate, J.A., 1991. Eruptive history of earth's largest Quaternary caldera (Toba, Indonesia) clarified. Geology 19, 200–203.

Cohen, A.S., Stone, J.R., Beuning, K.R.M., Park, L.E., Reinthal, P.N., Dettman, D., Scholz, C.A., Johnson, T.C., King, J.W., Talbot, M.R., Brown, E.T., Ivory, S.J., 2007. Ecological consequences of early Late Pleistocene megadroughts in tropical Africa. Proceedings of the National Academy of Science, USA 104, 16422–16437.

Collatz, J.G., Berry, J.A., Clark, J.S., 1998. Effects of climate and atmospheric CO_2 partial pressure on the global distribution of C_4 grasses: present, past and future. Oecologia 114, 441–454.

Collins, B.D., Dunne, T., 1986. Erosion of tephra from the 1980 eruption of Mount St. Helens. Geological Society of America Bulletin 97, 896–905.

Dansgaard, W., Johnsen, S.J., Clausen, H.B., Dahl-Jensen, D., Gundestrup, N.S., Hammer, C.U., Hvidberg, C.S., Steffensen, J.P., Sveinbjörnsdóttir, A.E., Jouzel, J., Bond, G., 1993. Evidence for general instability of past climate from a 250-kyr ice-core record. Nature 364, 218–220.

De Silva, S., 2008. Arc magmatism, calderas and supervolcanoes. Geology 36, 671–672.

Ehleringer, J.R., Cerling, T.E., Helliker, B.R., 1997. C_4 photosynthesis, atmospheric CO_2 and climate. Oecologia 112, 285–299.

Forster, P., 2004. Ice ages and the mitochondrial DNA chronology of human dispersals: a review. Philosophical Transactions of the Royal Society of London B 359, 255–264.

Gasparotto, G., Spadafora, E., Summa, V., Tateo, F., 2000. Contribution of grain size and compositional data from the Bengal Fan sediment to the understanding of Toba volcanic event. Marine Geology 162, 561–572.

Gates, A.E., Ritchie, D., 2007. Encyclopedia of Earthquakes and Volcanoes, 3rd edition. Facts on File, New York.

Gathorne-Hardy, F.J., Harcourt-Smith, W.E.H., 2003. The super-eruption of Toba, did it cause a human bottleneck? Journal of Human Evolution 45, 227–230.

Genty, D., Combourieu Nebout, N., Hatté, C., Blamart, D., Dhaleb, B., Isabello, L., 2005. Rapid climate changes of the last 90 kyr recorded on the European continent. Compte Rendus Geoscience 337, 970–982.

Goldberg, T.L., 1996. Genetics and biogeography of East African chimpanzees (*Pan troglodytes schweinfurthii*). Unpublished PhD Thesis, Harvard University.

Grootes, P.M., Stuiver, M., White, J.M.C., Johnsen, S., Jouzel, J., 1993. Comparison of oxygen isotope records from the GISP2 and GRIP Greenland ice cores. Nature 366, 552–554.

Gupta, S.K., Deshpande, R.D., 2005. Groundwater isotopic investigations in India: what has been learned? Current Science 89, 825–835.

Gupta, S.K., Deshpande, R.D., Bhattacharya, S.K., Jani, R.A., 2005. Groundwater $\delta^{18}O$ and δD from central Indian peninsula: Influence of the Arabian Seas and the Bay of Bengal branches of the summer monsoon. Journal of Hydrology 303, 38–55.

Haigh, J., Maynard Smith, J., 1972. Population size and protein variation in man. Genetical Research 19, 73–89.

Harpending, H.C., Sherry, S.T., Rogers, A.L., Stoneking, M., 1993. The genetic structure of ancient human populations. Current Anthropology 34, 483–496.

Hernandez, R.D., Hubisz, M.J., Wheeler, D.A., Smith, D.G., Ferguson, B., Ryan, D., Rogers, J., Nazareth, L., Indap, A., Bourquin, T., McPherson, J., Muzny, D., Gibbs, R., Nielsen, R., Bustamante, C.D., 2007. Demographic histories and patterns of linkage disequilibrium in Chinese and Indian rhesus macaques. Science 316, 240–243.

Johnsen, S.J., Dahl-Jensen, D., Gundestrup, N., Steffensen, J.P., Clausen, H.B., Miller, H., Masson-Delmotte, V., Sveinbjørndóttir, A.E., White, J., 2001. Oxygen isotope and paleotemperature records from six Greenland ice-core stations: Camp Century, Dye-3, GRIP GISP2, Renland and NorthGRIP. Journal of Quaternary Science 16, 299–307.

Jones, G.S., Gregory, J.M., Stott, P.A., Tett, S.F.B., Thorpe, R.B., 2005. An AOGCM model of the climate response to a volcanic super-eruption. Climate Dynamics 25, 725–738.

Jones, M.T., Sparks, R.S.J., Valdes, P.J., 2007. The climatic impact of supervolcanic ash blankets. Climate Dynamics 29, 553–564.

Jorde, L.B., Bamshad, M., Rogers, A.R., 1998. Using mitochondrial and nuclear DNA markers to reconstruct human evolution. BioEssays 20, 126–136.

Ke, Y., Su, B., Song, X., Lu, D., Chen, L., Li, H., Qi, C., Marzuki, S., Deka, R., Underhill, P., Xiao, C., Shriver, M., Lell, J., Wallace, D., Wells, R.S., Seielstad, M., Oefner, P., Zhu, D., Jin, J., Huang, W., Chakraborty, R., Chen, Z., Jin, L., 2001. African origin of modern humans in East Asia: a tale of 12, 000 Y chromosomes. Science 292, 1151–1153.

Kelly, P.M., Jones, P.D., Pengqun, J., 1996. The spatial response of the climate system to explosive volcanic eruptions. International Journal of Climatology 16, 537–550.

Kudrass, H.R., Hofmann, A., Doose, H., Emeis, K., Erlenkeuser, H., 2001. Modulation and amplification of climatic changes in the northern hemisphere by the Indian summer monsoon during the past 80 k.y. Geology 29, 63–66.

Landais, A., Masson-Delmotte, V., Combourieu Nebout, N., Jouzel, J., Blunier, T., Leuenberger, M., Dahl-Jensen, D., Johnsen, S., 2007. Millenial scale variations of the isotopic composition of atmospheric oxygen over Marine Isotope Stage 4. Earth and Planetary Science Letters 258, 101–113.

Lang, C., Leuenberger, M., Schwander, J., Johnsen, S., 1999. 16 ºC rapid temperature variation in central Greenland 70, 000 years ago. Science 286, 934–937.

Liu, Z., Colin, C., Trentesaux, A., 2006. Major element geochemistry of glass shards and minerals of the Youngest Toba Tephra in the southwestern South China Sea. Journal of Asian Earth Sciences 27, 99–107.

Louys, J., 2007. Limited effect of the Quaternary's largest super-eruption (Toba) on land mammals from southeast Asia. Quaternary Science Reviews 26, 3108–3117.

Luo, S.-J., Kim, J.-H., Johnson, W.E., van der Walt, J., Martenson, J., Yuhki, N., Miquelle, D.G., Uphyrkina, O., Goodrich, J.M., Quigley, H.B., Tilson, R., Brady, G., Martelli, P., Subramaniam, V., McDougal, C., Hean, S., Huang, S.-Q., Pan, W., Karanth, U.K., Sunquist, M., Smith, J.L.D., O'Brien, S.J., 2004. Phylogeography and genetic ancestry of tigers (*Panthera tigris*). PLoS Biology 2, 2275–2293.

Machette, M.N., 1985. Calcic soils of the southwestern United States. Geological Society of America Special Paper 203, 1–22.

Meese, D.A., Gow, A.J., Alley, R.B., Zielinski, G.A., Grootes, P.M., Ram, M., Taylor, K.C., Mayewski, P.A., Bolzan, J.F., 1997. The Greenland Ice Sheet Project 2 depth-age scale: Methods and results. Journal of Geophysical Research 102, 26411–26423.

Mellars, P., 2006. Going east: new genetic and archaeological perspectives on the modern human colonization of Eurasia. Science 313, 796–800.

Mountain, J.L., Cavalli-Sforza, L.L., 1997. Multilocus genotypes, a tree of individuals, and human evolutionary history. American Journal of Human Genetics 61, 705–718.

Mukhopadhyay, P.K., Ramachandra, H.N., 1997. Petrographic study of the Quaternary tephra occurrences of the Narmada Basin, Madhya Pradesh, India. Geological Survey of India, Special Publication 46, 79–85.

Ninkovich, D., Sparks, R.S.J., Ledbetter, M.T., 1978a. The exceptional magnitude and intensity of the Toba eruption, Sumatra: an example of the use of deep-sea tephra layers as a geological tool. Bulletin Volcanologique 41, 1–13.

Ninkovich, D., Shackleton, N.J., Abdel-Monem, A.A., Obradovich, J.D., Izett, G., 1978b. K-Ar age of the late Pleistocene eruption of Toba, north Sumatra. Nature 276, 574–577.

North Greenland Ice Project (NGRIP) Members (Anderson, K. K., Azuma, N., Barnola, J.-M., Bigler, M., Biscaye, P., Caillon, N., Chappellaz, J., Clausen, H.B., Dahl-Jensen, D., Fischer, H., Flückiger, J., Fritzsche, D., Fujii, Y., Goto-Azuma, K., Grønvold, K., Gundestrup, N.S., Hansson, M., Huber, C., Hvidberg, C.S., Johnsen, S.J., Jonsell, U., Jouzel, J., Kipfstuhl, S., Landais, A., Leuenberger, M., Lorrain, R., Masson-Delmotte, V., H. Miller, Motoyama, H., Narita, H., Popp, T., Rasmussen, S.O., Raynaud, D., Rothlisberger, R., Ruth, U., Samyn, D., Schwander, J., Shoji, H., Siggard-Andersen, M.-L., Steffensen, J.P., Stocker, T., Sveinbjörnsdóttir, A.E., Svensson, A., Takata, M., Tison, J.-L., Thorsteinsson, Th., Watanabe, O., F. Wilhelms, F., White, J. W. C.), 2004. High resolution record of northern hemisphere climate extending into the last interglacial period. Nature 431, 147–151.

Oppenheimer, C., 2002. Limited global change due to the largest known Quaternary eruption? Quaternary Science Reviews 21, 1593–1609.

Petraglia, M., Korisettar, R., Boivin, N., Clarkson, C., Ditchfield, P., Jones, S., Koshy, J., Lahr, M.M., Oppenheimer, C., Pyle, D., Roberts, R., Schwenniger, J.-C., Arnold, L., White, K., 2007. Middle Pleistocene assemblages from the Indian subcontinent before and after the Toba super-eruption. Science 317, 114–116.

Pattan, J.N., Shane, P., Banakar, V.K., 1999. New occurrence of Youngest Toba Tuff in abyssal sediments of the Central Indian Basin. Marine Geology 155, 243–248.

Rampino, M.R., Ambrose, S.H., 2000. Volcanic winter in the Garden of Eden: The Toba supereruption and the late Pleistocene human population crash. In: McCoy, F.W., Heiken, G. (Eds.), Volcanic Hazards and Disasters in Human Antiquity: Geological Society of America, Special Paper, vol. 345, pp. 71–82.

Rampino, M.R., Self, S., 1982. Historic eruptions of Tambora (1815), Krakatau (1883), and Agung (1963), their stratospheric aerosols, and climatic impact. Quaternary Research 18, 127–143.

Rampino, M.R., Self, S., 1992. Volcanic winter and accelerated glaciation following the Toba super-eruption. Nature 359, 50–52.

Rampino, M.R., Self, S., 1993. Climate-volcanism feedback and the Toba eruption of 74 000 years ago. Quaternary Research 40, 269–280.

Rampino, M.R., Stothers, R.B., Self, S., 1985. Climatic effects of volcanic eruptions. Nature 313, 372.

Richter, D., Tostevin, G., Škrdla, P., 2008. Bohunician technology and thermoluminescence dating of the type locality of Brno–Bohunice (Czech Republic). Journal of Human Evolution 55, 871-855.

Robock, A., Ammann, C.M., Oman, L., Shindell, D., Levis, S., Stenchikov, G., 2009. Did the Toba volcanic eruption of 74 ka B.P. produce widespread glaciation? Journal of Geophysical Research 114, D10107. doi:10.1029/2008JD011652.

Rose, W.I., Chesner, C.A., 1987. Dispersal of ash in the great Toba eruption, 75 ka. Geology 15, 913–917.

Rousseau, D.-D., Kukla, G., 2000. Abrupt retreat of summer monsoon at the S1/L1 boundary in China. Global and Planetary Change 26, 189–198.

Sadler, J.P., Grattan, J.P., 1999. Volcanoes as agents of past environmental change. Global and Planetary Change 21, 181–196.

Schulz, H., Emeis, K.-C., Erlenkeuser, H., von Rad, U., Rolf, C., 2002. The Toba volcanic event and interstadial/stadial climates at the marine isotope stage 5 to 4 transition in the northern Indian Ocean. Quaternary Research 57, 22–31.

Scholz, C.A., Johnson, T.C., Cohen, A.S., King, J.W., Peck, J.A., Overpeck, J.T., Talbot, M.R., Brown, E.T., Kaleindekafe, L., Amoako, P.Y.O., Lyons, R.P., Shanahan, T.M., Castañeda, I.S., Heil, C.W., Forman, S.L., McHague, L.R., Beuning, K.R., Gomez, J., Pierson, J., 2007. East African megadroughts between 135 and 75 thousand years ago and bearing on modern human origins. Proceedings of the National Academy of Science, USA 104, 16416–16421.

Shane, P., Westgate, J., Williams, M., Korisettar, R., 1995. New geochemical evidence for the Youngest Toba Tuff in India. Quaternary Research 44, 200–204.

Smith, B.N., Epstein, S., 1971. Two categories of 13C/12C ratios for higher plants. Plant Physiology 47, 380–384.

Smith, H.J., Whalen, M., Mastroianni, D., Taylor, K., Mayewski, P., 1997. The CO_2 concentration of air trapped in Greenland Ice Sheet Project 2 ice formed during periods of rapid climate change. Journal of Geophysical Research 102, 26577–26582.

Song, S.-R., Chen, C.-H., Lee, M.-Y., Yang, T.F., Iizuka, Y., Wei, K.-Y., 2000. Newly discovered eastern dispersal of the youngest Toba tuff. Marine Geology 167, 303–312.

Steiper, M.E., 2006. Population history, biogeography, and taxonomy of orangutans (Genus: *Pongo*) based on a population genetic meta-analysis of multiple loci. Journal of Human Evolution 50, 509–522.

Thalmann, O., Fischer, A., Lankester, F., Pääbo, S., Vigilant, L., 2007. The complex history of gorillas: insights from genomic data. Molecular Biology and Evolution 24, 146–158.

Tishkoff, S.A., Reed, F.A., Friedlaender, F.R., Ehret, C., Ranciaro, A., Froment, A., Hirbo, J.B., Awomoyi, A.A., Bodo, J.-M., Doumbo, O., Ibrahim, M., Juma, A.T., Kotze, M.J., Lema, G., Moore, J.H., Mortensen, H., Nyambo, T.B., Omar, S.A., Powell, K., Pretorius, G.S., Smith, M.W., Thera, M.A., Wambebe, C., Weber, J.L., Williams, S.D., 2009. The genetic structure and history of Africans and African Americans. Science 324, 1035–1044.

van der Kaars, S., Wang, X., Kershaw, P., Guichard, F., Setiabudi, D.A., 2000. A Late Quaternary palaeoecological record from the Banda Sea, Indonesia: patterns of vegetation, climate and biomass burning in Indonesia and northern Australia. Palaeogeography, Palaeoclimatology, Palaeoecology 155, 135–153.

Wang, D., Portis Jr., A.R., Moose, S.P., Long, S.P., 2008. Cool C_4 photosynthesis: Pyruvate P_i dikinase expression and activity corresponds to the exceptional cold tolerance of carbon assimilation in *Miscanthus x giganteus*. Plant Physiology 148, 557–567.

Ward, J.K., Myers, D.A., Thomas, R.B., 2008. Physiological and growth responses of C_3 and C_4 plants to reduced temperature when grown at low CO_2 of the last ice age. Journal of Integrative Plant Biology 50, 1288–1395.

Watson, E., Forster, P., Richards, M., Bandelt, H.-J., 1997. Mitochondrial footprints of human expansions in Africa. American Journal of Human Genetics 61, 691–704.

Weninger, B., Jöris, O., 2008. A 14C calibration curve for the last 60 ka: the Greenland-Hulu U/Th timescale and its impact on understanding the Middle to Upper Paleolithic transition in Western Eurasia. Journal of Human Evolution 55, 772–781.

Westgate, J.A., Shane, P.A.R., Pearce, N.J.G., Perkins, W.T., Korisettar, R., Chesner, C.A., Williams, M.A.J., Acharyya, S.K., 1998. All Toba tephra occurrences across peninsular India belong to the 75, 000 yr B.P. eruption. Quaternary Research 50, 107–112.

Wilmhurst, J.M., McGlone, M.S., 1996. Forest disturbance in the central North Island, New Zealand, following the 1850 BP Taupo eruption. The Holocene 6, 399–411.

Wilmhurst, J.M., Eden, D.N., Froggatt, P.C., 1999. Late Holocene forest disturbance in Gisborne, New Zealand: a comparison of terrestrial and marine pollen records. New Zealand Journal of Botany 37, 523–540.

Williams, M.A.J., Clarke, M.F., 1984. Late Quaternary environments in north central India. Nature 308, 633–635.

Williams, M.A.J., Clarke, M.F., 1995. Quaternary geology and prehistoric environments in the Son and Belan Valleys, north central India. Geological Society of India Memoir 32, 282–308.

Williams, M.A.J., Royce, K., 1982. Quaternary geology of the middle Son Valley, north central India: implications for prehistoric archaeology. Palaeogeography, Palaeoclimatology, Palaeoecology 38, 139–162.

Williams, M., Dunkerley, D., De Deckker, P., Kershaw, P., Chappell, J., 1998. Quaternary Environments, 2nd Edition. Arnold, London. 329 pp.

Williams, M.A.J., Pal, J.N., Jaiswal, M., Singhvi, A.K., 2006. River response to Quaternary climatic fluctuations: evidence from the Son and Belan valleys, north central India. Quaternary Science Reviews 25, 2619–2631.

Zielinski, G.A., Mayewski, P.A., Meeker, L.D., Whitlow, S., Twickler, M.S., 1996. Potential atmospheric impact of the Toba mega-eruption 71, 000 years ago. Geophysical Research Letters 23, 837–840.